On-line installation of the Superallowed Transition Beta-Neutrino Decay Ion Coincidence Trap

M. Brodeur^{1,*}, D.W. Bardayan¹, O. Bruce¹, R. Bualuan¹, D.P. Burdette², J.A. Clark², A.T. Gallant³, D. Gan¹, D. Guillet^{1,4}, A.M. Houff¹, J.J. Kolata¹, B. Liu¹, P.D. O'Malley¹, W.S. Porter¹, C. Quick¹, F. Rivero¹, G. Savard², W.W. von Seeger¹, A.A. Valverde², and R. Zite¹

Abstract. The Cabibbo-Kobayashi-Maskawa quark mixing matrix currently does not satisfy unitarity at the 2σ -level. This could be the result of an inaccurate value of one or both of its largest matrix elements V_{us} and V_{ud} . In the case of V_{ud} , the most precise measurement is obtained from the ft-value measurements of superallowed beta-transitions between 0⁺ states. The accuracy of this determination can, in turn, be tested by extracting V_{ud} in other transitions including superallowed transitions between mirror nuclei. The Superallowed Transition Beta-Neutrino Decay Ion Coincidence Trap (St. Benedict) is currently under construction at the Nuclear Science Laboratory of the University of Notre Dame to perform such a determination, with the goal of shedding more light on this tension with unitarity. St. Benedict will take a radioactive ion beam produced by TwinSol, thermalize it in a large volume gas catcher, then transport it in two separate differentially-pumped volumes using a radio-frequency (RF) carpet and a radio-frequency quadrupole (RFQ) ion guide before injecting it in an RFQ trap to create cool ion bunches for injection in the measurement Paul trap. In this paper, we detail the installation of the beam preparation components of St. Benedict, and present the results of the first RIBs successfully stopped and extracted from its gas catcher.

1 Introduction

The Standard Model has, for several decades, persisted in successfully describing fundamental particles and their interactions [1]. This model is known to be incomplete as it does not include gravity, dark matter, nor explain the matter-antimatter asymmetry in the universe. Hence it is continuously being scrutinized not only in the high-energy regime but also in the low-energy regime via precision measurements of electric dipole moments [2] and nuclear beta-decays [3]. The latter includes searches for beyond the Standard Model scalar and tensor currents and unitarity tests of the Cabibbo-Kobayashi-Maskawa (CKM) quark mixing matrix [4]. The Standard Model prediction of CKM matrix unitarity has been under tension

¹Department of Physics, University of Notre Dame, Notre Dame, IN, USA

²Physics Divison, Argonne National Laboratory, Argonne, IL, USA

³Nuclear and Chemical Sciences Division, Lawrence Livermore National Laboratory, Livermore, CA, USA

⁴École normale supérieure Paris-Saclay, France

^{*}e-mail: mbrodeur@nd.edu

since new transition-independent radiative corrections lowered the value of its largest element, V_{ud} [5]. Simultaneously, the other large top-row element, V_{us} , is not on solid footing either, as its determination strongly depends on the type of kaon decay under consideration [6]. Hence, there are currently large experimental and theoretical efforts underway to solidify the determination of both of these elements [4, 6].

The V_{ud} matrix element can be obtained from the superallowed beta-decay transitions of the pion, the neutron, and nuclear decays between either 0^+ states or mirror nuclei [7], each with their own drawbacks. The pion beta-decay has a very small branching ratio making the extraction of V_{ud} statistics-limited [8]. The determination from neutron decay suffers from the neutron lifetime anomaly [9, 10] and inconsistent determination of the required ratio of vector-to-axial-vector coupling constants [11, 12]. Nuclear decays require the use of theoretical corrections to account for the presence of other nucleons during the decay. However, many isotopes undergo such a decay, which helps ensure a consistent and accurate determination of V_{ud} from these decays, collectively [13]. In fact, the determination of V_{ud} from 0^+ decays is by far the most precise [14]. Currently, the precision of V_{ud} from 0^+ decays is limited by the theoretical correction terms, hence a primary focus to help probe the tension in CKM unitarity is on promoting improved calculation techniques for these corrections.

One avenue to test the prediction of various calculation methods is via the determination of V_{ud} from superallowed beta-decay transitions between mirror nuclei. Unfortunately this type of decay requires an additional parameter, the Fermi-to-Gamow-Teller mixing ratio, ρ , to extract V_{ud} . Presently this value is only sufficiently well known in 5 mirror nuclides [15]. As such, the Superallowed Transition Beta-Neutrino Decay Ion Coincidence Trap (St. Benedict) [16] is currently under construction at the University of Notre Dame Nuclear Science Laboratory (NSL). The goal of this system is to determine ρ via a measurement of the $\beta - \nu$ angular correlation parameter $a_{\beta\nu}$ in several superallowed beta-decay transitions between mirror nuclei ranging from 11 C to 41 Sc, many of which will be measured for the first time. This article will present St. Benedict and give an update on its construction and commissioning.

2 Online installation of St. Benedict

St. Benedict is located in the Far West Target Room (FWTR) of the NSL along the zero-degree beamline downstream of a 15-degree switching magnet. The other neighboring line provides beams to the TriSol [17] magnet (see figure 1). The FWTR beamlines take radioactive ion beams (RIBs) from the *TwinSol* facility [18] located in an upstream target vault. The components of St. Benedict currently installed (see figure 1) include a large-volume gas catcher that thermalize the incoming 10-40 MeV beams from *TwinSol*, a differential pumping extraction system comprise a radio-frequency (RF) carpet and a radio-frequency quadrupole (RFQ) ion guide, and a RFQ cooler-buncher. Only the linear Paul trap, where measurements of $a_{\beta\nu}$ will take place, remains to be installed. The function and status of each component are given below.

2.1 Gas catcher

The St. Benedict gas catcher plays the crucial role of converting the in-flight-produced fast beams from TwinSol into slow beams that can be used for trapping experiments. In order to accomplish this, the RIBs must first lose the majority of their kinetic energy by passing through a 7- μ m-thick Al degrader (figure 2), which is mounted on a rotating actuator, and a 12.5 μ m foil that acts as the entrance window to the gas volume. The rest of the beam energy is lost via collisions with the helium atoms in the 25-75-mbar-pressure gas volume of

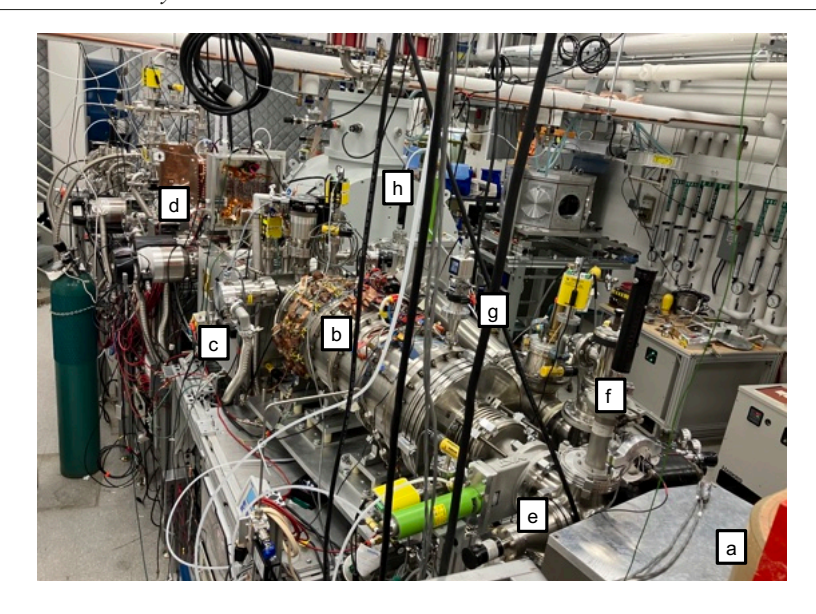


Figure 1. Far West Target Room beamlines downstream of the 15 degrees switching magnet (a). The St. Benedict gas catcher (b), extraction chamber (c), and cooler-buncher (d) as well as the location of the degrader (e) and beam tuning silicon detector (f) are indicated. The adjacent 15 degrees beamline (g) leading to the TriSol magnet (h) is also shown.

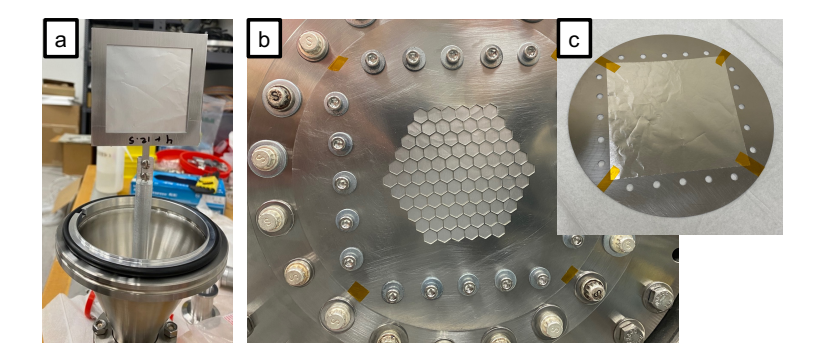


Figure 2. a) The 7 μ m-thick aluminum degrader mounted on a 7-cm-wide aluminum frame and attached to its rotating actuator. b) The honeycomb-shaped supporting mesh for the gas catcher window. c) The 12.5- μ m-thick aluminum window.

the catcher. The walls of the gas catcher are lined with a series of closely-spaced, washer-shaped electrodes over which a potential gradient can be applied, resulting in the creation of an electric field that drags the thermalized ions through the volume. Towards the end of the gas catcher, the diameter of these electrodes decreases, forming a conical funnel that helps guide the ions towards an exit 1.6-mm-diameter nozzle. These electrodes also receive an alternating RF signal with opposite polarity on adjacent electrodes to generate a repelling force and, in combination with the potential gradient, help corral the ions towards an exit nozzle sitting at ground potential. Once the ions are in close proximity to the nozzle, the

large pressure difference between the gas catcher and following chamber results in a large gas flow that rapidly extracts the ions.

The gas catcher was previously used at Argonne National Laboratory and in 2022 was moved to the University of Notre Dame where its RF circuits received minor repairs and were impedance-matched. The gas catcher has been leak-checked and evacuated down to below 3×10^{-8} mbar. After, the transport of potassium ions produced by a thermionic source has been demonstrated at pressures of up to 100 mbar. The gas catcher has recently been installed in the FWTR, as shown in figure 1, and commissioned with various RIBs from *TwinSol*. These results are presented in Sect. 3.

2.2 Extraction system

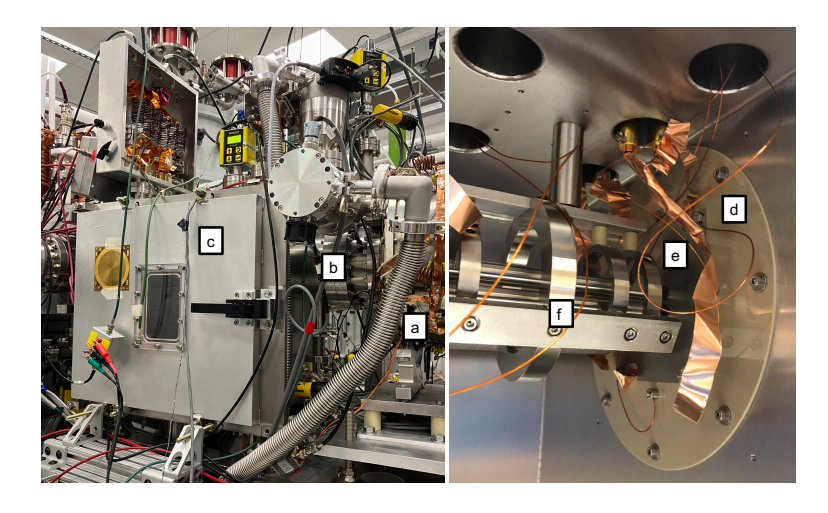


Figure 3. Left: Exterior of the differently-pumped extraction system. a) Exit end of the gas catcher b) Small chamber housing the RF carpet c) Large chamber housing the RFQ ion guide and 90 degrees ion source. Right: Inside the large chamber. d) PEEK sheet partitioning the two chambers. e) RF carpet aperture. f) Ion guide structure.

The extraction system comprise two differently-pumped chambers which allow for the evacuation of the helium exiting the gas catcher's nozzle and the transport of the thermalized ions. The first chamber (see figure 3) is 23.6-cm-long and held at a pressure in the 1-6 mbar range, depending on the pressure in the gas catcher, using an Ecodry 65 plus pump. The wall opposite to the nozzle features an RF carpet with a 0.74-mm-diameter hole at its center [19]. The RF carpet is at a negative potential, which generates an electric field that pulls the ions to it from the nozzle. The carpet is formed by a series of concentric goldplated copper rings on a kapton substrate. Each electrode receives two time-varying signals of different frequency. The first one, at 12.6 MHz and with an amplitude of, at most 70 V, is phase-shifted by 180 degrees between adjacent electrodes, and results in the creation of a repelling force that pushes the ions away from the carpet surface. The second signal is at a lower frequency of 50 kHz, with 1.5 V amplitude, and phase-shifted by 90 degrees between adjacent electrode, producing a traveling wave that transports the hovering ions towards the central hole. The RF carpet is mounted on a PEEK sheet that serves as a differential pumping barrier with the subsequent chamber (see figure 3). On the other side of this sheet a stainless steel plate with a cylindrical-shaped tube protrudes into the hole of the PEEK sheet. This

electrode, referred to as the "RF carpet aperture", is at a lower potential than the RF carpet to generate an electric field that helps extract the ions towards the subsequent chamber. Prior to its on-line installation, the RF carpet has been tested by transporting potassium ions produced by a thermionic source. Complete ion transport for pressures in the range 0.75-6 mbar have been demonstrated [20].

The second chamber (see figure 3) houses a 395-mm-long ion guide that transports the ions extracted from the RF carpet at a pressure in the 10^{-3} mbar range maintained by one 350 L/s and one 260 L/s turbomolecular pump. The ion guide consists of three sections of four cylindrical, 9.5-mm-diameter, rods that form an inscribed radius of 4.2 mm. The two outer sections are 188.5-mm-long each while the central section is only 18 mm long. Perpendicular to the central section, a thermionic ion source is installed to produce a stable ion beam which is injected from a 90 degree angle into the system. The operation frequency of the ion guide is typically 4.3 MHz with an amplitude of 290 V. Downstream of the ion guide a 4-mm-thick, stainless steel aperture with a 6-mm-diameter hole is mounted on a PEEK sheet that serves as a differential pumping barrier. This aperture electrode, along with the segmented rods allow for the application of a potential gradient which gently pulls the ions through this component. The ion guide has been tested off-line, in combination with the RF carpet, and an overall transport efficiency of potassium ions reaching 70% has been achieved. Transport of ions from the 90 degree ion source has also been demonstrated.

2.3 Cooler-buncher

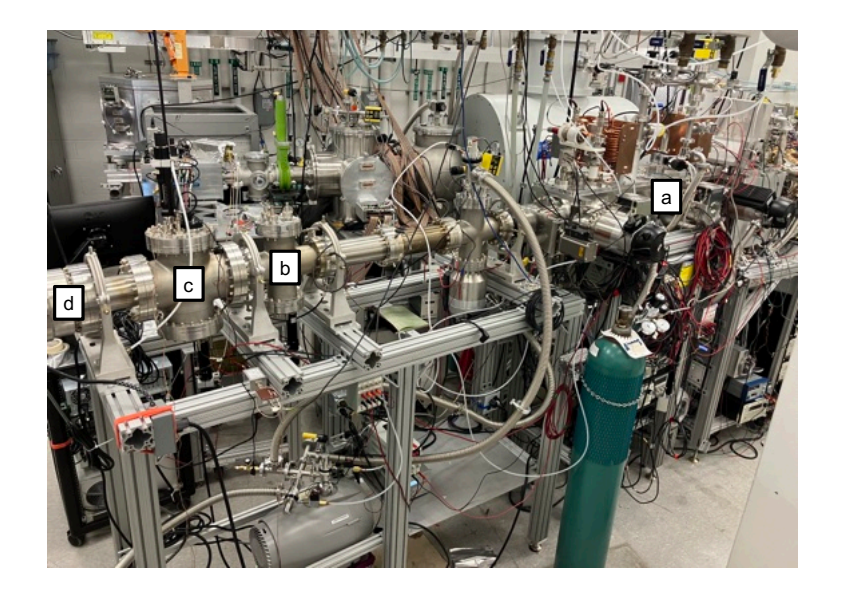


Figure 4. RFQ cooler buncher (a) and beamline connecting to the future Paul trap. Indicated are the crosses containing b) the silicon detector and Bradbury-Nielsen gate and c) the micro channel plate detector. d) Turbo molecular pump temporarily located at the future entrance to the linear Paul trap.

The dynamic trapping of ions in the measurement Paul trap requires ion bunches with small energy and temporal spread. The production of such bunches from the continuous ion beam is accomplished by the RFQ cooler-buncher [21]. The ion beam from the extraction system is first focused at the entrance of the cooler-buncher using an Einzel lens. Upon

entering the device, the beam is radially confined using a tapered RFQ structure that brings the ions into a region at a helium pressure in the 10^{-2} -mbar-range. There, the ions are cooled via collisions with helium while remaining radially confined by the RFQ electrodes, which are segmented to produce a longitudinal drag potential. At the exit of the cooling region, the segmented quadrupole electrodes are used to create a potential well, which allows the accumulation and settling of the cooled ions After a given time the beam is blocked at the entrance of the device and the bunch of ions is released by rapidly switching the potentials on the electrodes adjacent to the well. The RFQ cooler-buncher was commissioned offline using a potassium ion source and has now been installed and aligned downstream of gas catcher and extraction system. Figure 4 shows the cooler-buncher and the following beamline that will bring the bunches to the Paul trap. This beamline includes a silicon detector to measure the transported activity, a Bradbury-Nielsen gate to separate potential non-isobaric radioactive contamination by time-of-flight as well as a micro-channel plate detector and a Faraday cup for beam tuning.

2.4 Linear Paul trap

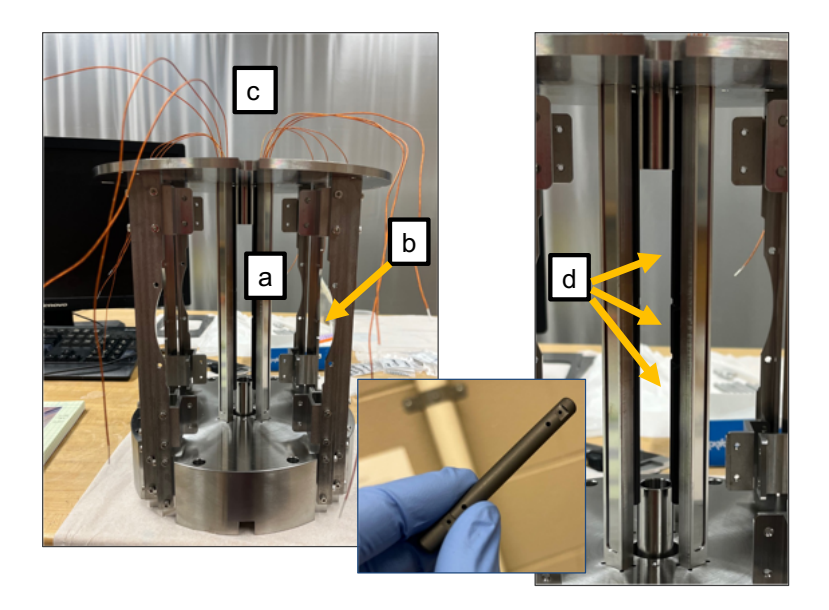


Figure 5. Left: a) Frame holding the linear Paul trap and b) one of the four holes that will contain detectors. c) Wires carrying the combined RF and DC signals. Right: Linear Paul trap with the segmented quadrupoles indicated (d). Bottom: one of the graphite rods forming the quadrupole.

The linear Paul trap, shown in figure 5, is the last component that remains to be installed on-line and it is where the measurement will take place. The bunches of radioactive ions will be confined radially by the application of a RF signal on its quadrupole structure. These rods are segmented into three sections that allow for the creation of a potential well for the axial confinement. A small amount of helium (in the 10^{-6} -to- 10^{-5} -mbar-range) will be injected to cool the ion cloud and provide a smaller ion cloud size. The trap will be surrounded by two double-sided silicon strip detectors (DSSD) placed at 90 degrees from one another and, facing them, two position-sensitive micro channel plate (MCP) detectors with resistive anodes. The DSSDs will provide position information on the emitted positron. They will be

backed by plastic scintillators attached to photomultiplier tubes for timing and energy information. The MCPs, on the other hand, will provide position and timing information of the recoiling daughter nuclei. The main measurement quantity of interest is the time difference between the signals from the beta and the daughter nuclei (TOF). The position information of the charged decay products and the energy of the beta particle will be used to suppress background and provide systematic checks. The $\beta - \nu$ angular parameter of the radioactive isotope being sampled will be determined by fitting the TOF distribution. The RF and DC circuit and the linear Paul trap itself have been constructed and tested. All detectors and the chamber that will contain the linear Paul trap have been received.

3 First stopping of RIBs for St. Benedict

RIB	Primary beam	Terminal voltage (MV)	RIB energy (MeV)
¹¹ C(6+)	$^{10}B(4+)$	6.60	23.0
$^{13}N(7+)$	$^{12}C(5+)$	6.97	28.6
$^{15}O(8+)$	$^{14}N(5+)$	8.50	33.9
$^{17}F(9+)$	$^{16}O(6+)$	8.76	39.8

Table 1. Properties of the RIBs sent to St. Benedict.

The gas catcher and its extraction system have been commissioned with four different RIBs from TwinSol listed in table 1. These settings were based on LISE++ [22] simulations assuming a 7- μ m-thick aluminum degrader, a 12.5 μ m aluminum window, 40 mbar of helium, and 410-430 mm of stopping range in helium. For all of these beams, a production target of deuterium gas at a pressure of ~1067 mbar was used. Before injection into St. Benedict, the different RIBs were identified by their total energy deposited in a silicon surface barrier detector that was inserted in front of the degrader. In future experiment the beam will be first send to ACKBAR [23], a combination ionization chamber (for the ΔE) and surface barrier (to measure the residual energy). This will provide a way to relate the particle identification to the total energy from the other surface barrier detector. Following beam purification with TwinSol, the RIBs were injected into the gas catcher and their stopping was studied as function of degrader angle.

Depending on the degrader angle the RIB will face a different effective thickness of degrader material and as a result lose more or less energy as it travels through it. At small angles the effective thickness is minimized and the RIB will enter the gas catcher with more energy. When the ion beam enters the gas catchers it typically has about 1 MeV of energy, and as such it ionizes a large number of helium atoms before it thermalizes. The electrons released from the ionization are drawn towards the window of the gas catcher since it is the region of the chamber that is at the highest potential. At small degrader angles the ion beam will lose the least amount of energy in the degrader and as a result will travel further in the gas catcher before coming to a stop. This will result in greater helium ionization, and therefore greater electron current recorded on the window as shown in figure 6 for ¹³N. At larger angles, greater than 60 degrees, the current increases again, as the degrader does not fully cover the beam profile and some of the beam enters the gas catcher untouched by the degrader. Figure 6 also shows the extracted ion beam current on the RF carpet as function of the degrader angle. This current follows nearly the same profile as the ionization electron current, indicating that both currents are emblematic of the ions stopping in the He gas. The current recorded on the RF carpet could be ionized helium near the nozzle or residual contaminants that charge-exchange

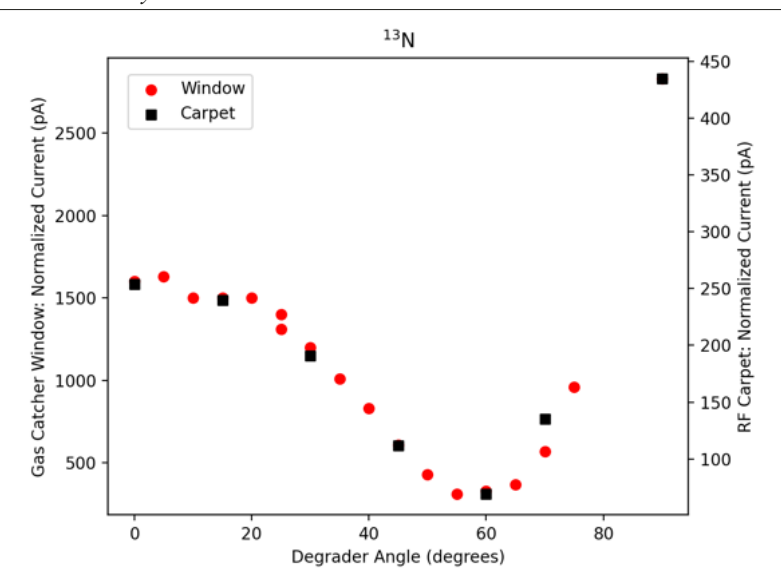


Figure 6. Electron current on the gas catcher window and ion beam current on the RF carpet as function of the degrader angle for ¹³N.

with the helium ions. The exact composition of the extracted beam will be studied in a future experiment by detection downstream of the cooler-buncher. Figure 4 shows the location of a silicon detector that will be used to confirm the extraction of the stopped RIB and count its activity. Further down the beamline an MCP detector will be used to analyze the beam composition by time-of-flight.

4 Conclusion

The St. Benedict system aims at measuring the $\beta - \nu$ angular correlation parameter in many superallowed beta-decay transitions between mirror nuclei for the first time. These measurements will allow the determination of these decays' Fermi-to-Gamow-Teller mixing ratio and enable tests of the theoretical corrections required for the extraction of the V_{ud} matrix element. The system comprises several essential components: a gas catcher to stop the fast RIB from TwinSol, an extraction system consisting of a RF carpet and RFQ ion guide to transport the extracted ions through a differentially-pumped region, a RFQ cooler-buncher, and a linear Paul trap where the measurement will take place. All devices except for the linear Paul trap have been installed on-line, downstream of the TwinSol RIB facility. The gas catcher has received its first RIBs and demonstrated its ability to stop and extract ion beams. The next step will consist of recommissioning the installed cooler-buncher and the following beamline using beams from off-line ion sources. Once this has been completed, the composition of the stopped beam, and any contaminants will be analyzed by looking at the activity on a silicon detector and the TOF of ion bunches on a MCP detector, both downstream of the cooler buncher. Finally, the linear Paul trap will be installed and tested with RIBs before performing its first angular correlation measurement.

Acknowledgement

This work was conducted with the support of the National Science Foundation under Grants PHY-1725711, PHY-2011890, PHY-2310059, and of the University of Notre Dame.

References

- [1] R.L. Workman, Others (Particle Data Group), PTEP **2022**, 083C01 (2022)
- [2] J. Engel, M.J. Ramsey-Musolf, U. van Kolck, Progress in Particle and Nuclear Physics **71**, 21 (2013), fundamental Symmetries in the Era of the LHC
- [3] M. González-Alonso, O. Naviliat-Cuncic, N. Severijns, Progress in Particle and Nuclear Physics **104**, 165223 (2019)
- [4] M. Gonzalez-Alonso, O. Naviliat-Cuncic, N. Severijns, Progress in Particle and Nuclear Physics **104**, 165 (2019)
- [5] C.Y. Seng, M. Gorchtein, H.H. Patel, M.J. Ramsey-Musolf, Phys. Rev. Lett. 121, 241804 (2018)
- [6] V. Cirigliano, A. Crivellin, M. Hoferichter, M. Moulson, Physics Letters B 838, 137748 (2023)
- [7] J.C. Hardy, I.S. Towner, Reports on Progress in Physics 73, 046301 (2010)
- [8] D. Pocanic, SciPost Phys. Proc. p. 024 (2021)
- [9] A.T. Yue, M.S. Dewey, D.M. Gilliam, G.L. Greene, A.B. Laptev, J.S. Nico, W.M. Snow, F.E. Wietfeldt, Phys. Rev. Lett. 111, 222501 (2013)
- [10] F.M. Gonzalez, E.M. Fries, C. Cude-Woods, T. Bailey, M. Blatnik, L.J. Broussard, N.B. Callahan, J.H. Choi, S.M. Clayton, S.A. Currie et al. (UCNτ Collaboration), Phys. Rev. Lett. 127, 162501 (2021)
- [11] M. Beck, W. Heil, C. Schmidt, S. Baeßler, F. Glück, G. Konrad, U. Schmidt, Phys. Rev. Lett. 132, 102501 (2024)
- [12] B. Märkisch, H. Mest, H. Saul, X. Wang, H. Abele, D. Dubbers, M. Klopf, A. Petoukhov, C. Roick, T. Soldner et al., Phys. Rev. Lett. 122, 242501 (2019)
- [13] J.C. Hardy, I.S. Towner, Phys. Rev. C 102, 045501 (2020)
- [14] A. Falkowski, M. González-Alonso, O. Naviliat-Cuncic, N. Severijns, The European Physical Journal A **59**, 113 (2023)
- [15] O. Naviliat-Cuncic, N. Severijns, Phys. Rev. Lett. **102**, 142302 (2009)
- [16] M. Brodeur, T. Ahn, D. Bardayan, D. Burdette, J. Clark, A. Gallant, J. Kolata, B. Liu, P. O'Malley, W. Porter et al., Nuclear Instruments and Methods in Physics Research Section B: Beam Interactions with Materials and Atoms 541, 79 (2023)
- [17] T. Ahn, D. Bardayan, D. Blankstein, C. Boomershine, M. Brodeur, S. Carmichael, S. Coil, J. Kolata, P. O'Malley, W. Porter et al., Nuclear Instruments and Methods in Physics Research Section B: Beam Interactions with Materials and Atoms 541, 216 (2023)
- [18] F. Becchetti, M. Lee, T. O'Donnell, D. Roberts, J. Kolata, L. Lamm, G. Rogachev, V. Guimarães, P. DeYoung, S. Vincent, Nuclear Instruments and Methods in Physics Research Section A: Accelerators, Spectrometers, Detectors and Associated Equipment 505, 377 (2003), proceedings of the tenth Symposium on Radiation Measurements and Applications
- [19] C. Davis, O. Bruce, D. Burdette, T. Florenzo, B. Liu, J. Long, P. O'Malley, M. Yeck, M. Brodeur, Nuclear Instruments and Methods in Physics Research Section A: Accelerators, Spectrometers, Detectors and Associated Equipment 1031 (2022)

- [20] C. Davis, R. Bualuan, O. Bruce, D. Burdette, A. Cannon, T. Florenzo, D. Gan, J. Harkin, B. Liu, J. Long et al., Nuclear Instruments and Methods in Physics Research Section A: Accelerators, Spectrometers, Detectors and Associated Equipment 1042, 167422 (2022)
- [21] A.A. Valverde, M. Brodeur, D.P. Burdette, J.A. Clark, J.W. Klimes, D. Lascar, P.D. O'Malley, R. Ringle, G. Savard, V. Varentsov, Hyperfine Interactions **240**, 38 (2019)
- [22] O. Tarasov, D. Bazin, M. Hausmann, M. Kuchera, P. Ostroumov, M. Portillo, B. Sherrill, K. Tarasova, T. Zhang, Nuclear Instruments and Methods in Physics Research Section B: Beam Interactions with Materials and Atoms 541, 4 (2023)
- [23] J. Long, C.R. Nicoloff, D.W. Bardayan, F.D. Becchetti, D. Blankstein, C. Boomershine, D.P. Burdette, M.A. Caprio, L. Caves, P.J. Fasano et al., Phys. Rev. C 106, 045501 (2022)